AIAA JOURNAL
Vol. 40, No. 2, February 2002

Prediction of Compressive Failure in Laminated Composites at Room and Elevated Temperature

Junghyun Ahn* and Anthony M. Waas†
University of Michigan, Ann Arbor, Michigan 48109-2140

An experimental and analytical investigation of the notched strength of fiber reinforced polymer matrix composite laminates subjected to remote uniaxial and biaxial loads is presented. Experimental results pertaining to failure mechanisms, critical loads, and critical strains for cross-ply and quasi-isotropic laminates at room and elevated temperature (200°C) are presented. A micromechanics based finite element analysis that uses readily available constituent properties for predicting notched strength of general multilayered composite laminates is developed and used to predict the experimentally measured failure loads. Good agreement between experiment and analysis is reported. The present methodology is an attempt to remove the empirical nature of composite strength prediction.

Introduction

LAMINATED fiber-reinforced polymer matrix composites (PMCs) are finding increased use in a broad range of industrial applications. Applications in the national infrastructure (such as all-composite bridges over interstate highways), the automotive industry, the medical sector, and the aerospace industry are some examples of where these materials are earmarked for several uses.

Composite materials are superior to conventional monolithic materials for a number of reasons, noteworthy among these being their mechanical properties. Ashby and Jones[1] have formulated performance indices that can be used to select a material for a given application based on satisfying certain objective measures. PMCs appear to be the material of choice for a number of such applications. Issues such as damage tolerance and durability, performance degradation due to aging, fatigue under multiaxial loads, and response at elevated temperature are currently being researched.

Experience with previous applications of PMCs for rotor blades in the helicopter industry, pressure vessels, and other similar situations that call for superior tensile stiffness and tensile fatigue life have shown PMCs superior performance in a tensile load environment. In contrast, the compressive strength of PMCs is known to be less attractive.[2,3]

The response of composite laminates when subjected to mechanical loads is influenced by the material type (fiber and matrix) and configuration (stacking sequence and layup). In addition to these factors, geometrical parameters (notches and thickness discontinuities) and loading characteristics (multiaxial, thermal, cyclic loading, to name a few) also affect the overall performance of composite laminates. One of the challenging tasks in the analysis and design of PMC-based structural laminates is to improve strength prediction, particularly for situations involving nonhomogeneous stress states[4] under different design environments.

Previous work related to the present investigation was undertaken by Sandhu,[5] Daniels et al.,[6] Soutis et al.,[7] Martin et al.,[8] and Wham and Palazotto.[9] Martin et al.[8] investigated failure in thermoplastic laminates and provided comparisons between theory and experiment. The effect of a central notch on failure in thermoplastic laminates was examined by Daniels et al.[6] and Wham and Palazotto.[9] In addition to these investigations, Waas and Schultheisz[3] provide a comprehensive review of previous work related to compressive failure in composite laminates.

The organization of the present paper is as follows. First, details of the uniaxial and biaxial experiments conducted on notched planar composite laminates will be presented. Results obtained from examining different types of laminates will be described, with important observations deduced from the tests to ascertain the laminate residual stiffness properties. This is followed by a discussion of the effect of the environment on the observed failure mode. Next, the development of a micromechanics-based finite element model to predict the onset of failure in notched laminated composites at room and elevated temperature, when subjected to remote planar uniaxial and biaxial loads, is presented. Both material degradation (due to temperature) and structural (stress concentration) effects are accounted for in the analysis. The predictions of the model are found to be in good agreement with the measured experimental results.

Details of the Experiments

Khamseh and Waas[10] have pointed out difficulties associated with stress concentrations that are encountered in the design of a cruciform-shaped planar specimen for in-plane biaxial loading of composite laminates. To select the size of the specimen in the present experiments, a model of the notched laminated plate and grips (steel) was generated using the ABAQUS® finite element analysis (FEA) software package. This stress analysis program was used to examine the effect of several specimen geometries on the stress concentrations due to the applied loads. The loads were applied at the boundaries of the loading arms by use of displacement constraints. Eight noded parabolic plane stress elements were used to model the plate material and steel grips. Ply properties were entered from which ABAQUS calculates the equivalent plane stress constants using classical lamination theory. From the results of the FEA, it was concluded that a cruciform configuration matching the dimensions given in Fig. 1 was the desirable specimen shape. The word "desirable" is used to identify with a stress state for which an in-plane region in the interior of the specimen (shown as the crosshatched area in Fig. 1) is not influenced by the effects of the far-field edges (i.e., edge curvatures identified as R_c in Fig. 1) due to the loading.

Several specimen configurations corresponding to different values of R_c were studied[10] using the FEA. The results were used to arrive at an optimum value of R_c based on the condition that the specimen with a hole does not contain effects associated with the stress concentration at the hole interfering with nonuniformities in the stress field generated on account of the edge curvatures. For the composite plate we studied, this working area translated into a 6.35-cm (2.5-in.) square region in the middle of the cruciform configuration.

The test specimens were made of graphite/toughened epoxy material containing Hercules IM7 (intermediate modulus) fiber and

Received 3 November 2000; revision received 10 July 2001; accepted for publication 11 July 2001.

*Research Fellow, Composite Structures Laboratory, Department of Aerospace Engineering. Member AIAA.

†Professor, Composite Structures Laboratory, Department of Aerospace Engineering. Associate Fellow AIAA.

Table 1 Zero-ply material properties of the 48-ply graphite/977-3 epoxy composites

Material	E_{11}, Msi/GPa	E_{22}, Msi/GPa	G_{12}, Msi/GPa	ν_{12}	Thickness, in. (mm)
IM7/977-3 epoxy	23.5/162.0	1.21/8.3	0.72/5.0	0.30	0.0052 (0.132)
IM7 fiber	42/289.6	——	——	0.25	$2.756E-04$ (0.007)
977-3 epoxy	0.7/4.8	——	——	0.34	$2.444E-04$ (0.006)

Table 2 Laminate material properties as determined from CLT using the properties from Table 1

Laminate type	Stacking sequence	E_{xx}, Msi/GPa	E_{yy}, Msi/GPa	G_{xy}, Msi/GPa	ν_{xy}
Quasi isotropic	$[+45/0/-45/90]_{6s}$	8.828/60.867	8.828/60.867	3.372/23.249	0.309
Cross ply	$[0/90]_{12s}$	12.401/85.502	12.404/85.502	0.7119/4.908	0.029

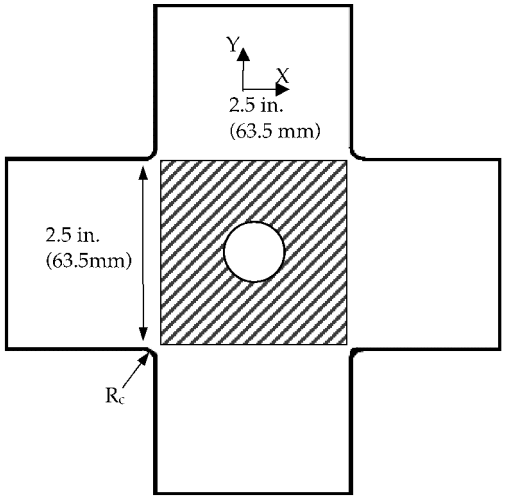

Fig. 1 Specimen configuration and dimensions. 5.5 in. (139.7 mm) × 5.5 in. (139.7 mm) cruiciform specimens, R_c = 0.25 in. (6.35 mm), HERCULES IM-7/977-3 (toughened epoxy resin), 48-ply plate, 0.5-in. (12.7-mm) hole diameter, 0.25-in. (6.35-mm) thickness, cross-ply: $(0/90)_{12s}$, and quasi-isotropic: $(+45/0/-45/90)_{6s}$.

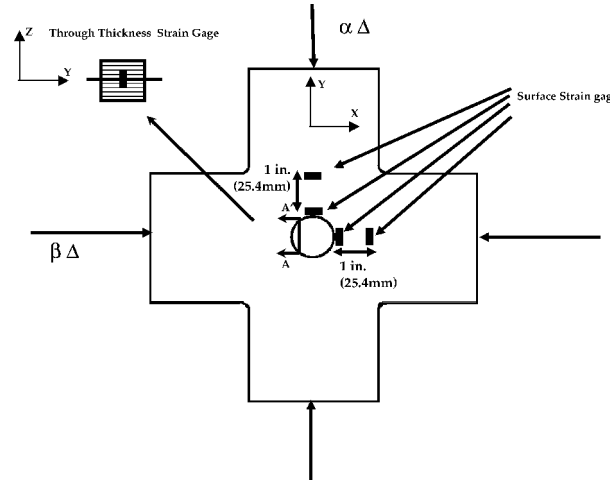

Fig. 2 Strain gauge locations on the specimen.

977-3 toughened epoxy matrix, designed for operation at elevated temperatures. In Table 1, the lamina properties are given, based on data provided by the manufacturer. Two types of stacking sequences were investigated: cross ply $[0/+90]_{12s}$ and quasi isotropic $[+45/0/-45/90]_{6s}$. In Table 2, Laminate material properties, calculated using generalized classical lamination theory (CLT) are listed. The linear elastic plane stress solution that corresponds to the present configuration, as given by Lekhnitskii,[11] was used to calculate the stress field corresponding to the uniaxial and equibiaxial loading used in the experiments. This solution were verified with the strain data (away from and near the hole edge) that were recorded in the room temperature test for each laminate type. Such a check yielded good agreement between test data and the two-dimensional elasticity solution. The details of the elasticity solution, the biaxial load frame used for the experiments, and the test procedure are given by Ahn.[12]

The in-plane dimensions of the test specimens are given in Fig. 1. The thickness of the laminates was 0.635-cm (0.25-in.) with a 0.013-cm (0.005-in.) tolerance. In the center of the steel grips, a 0.724-cm (0.285-in.) channel, 3.048 cm (1.200 in.) in depth, was machined along the length of the grip. The specimen was bonded to the walls of this channel with the use of Devcon® brand plastic steel putty adhesive, treated with release agent to allow for ease of separation of the two materials at the end of an experiment. The Devcon putty acts as an interface between the specimen edge and the surface on which the specimen sits, effectively smoothening out the interface surface irregularities between the two materials and ensuring a smooth load transfer.

To perform a compression test at elevated temperature, a feedback-controlled radiation-heating element with an insulation tunnel was designed. Special strain gauges for high temperature were used for the test. To ensure a steady temperature in the enclosed test chamber, four locations in the test chamber were used to monitor temperature. The heating rate was limited to be very slow (2°C/min). In addition, thermocouple gauges placed inside the specimen cutout edge and on the specimen surface were used to verify that the specimen temperature was fairly even (less than 1°C change from location to location). Circulating water through a copper pipe wrapped around both parts cooled the load cell and the loading frame. The maximum temperature of the tests was limited to 200°C (392°F).

A 50,000-lbf load cell was used to obtain a load time history of the far field applied load. Surface strain measurements at various locations on the specimen were obtained via strain gauges. Strain gauges were mounted along the edges of the hole, as well as in the corresponding far-field region. A set of two additional strain gauges were mounted inside the hole, along the wall thickness, to record changes in strain in the out-of-plane (through-the-thickness) direction, revealing failure initiation. Strain gauge locations are shown in Fig. 2. Strain gauge readings, along with load cell readings, were monitored and recorded using a commercial data analysis software package. The data sampling rate was five samples per second at a loading rate of 0.0001 in./s.

Experimental Procedure

The 48-ply composites were tested under uniaxial and 1:1 (in far-field displacement) biaxial loading at both room temperature (21°C) and 200°C to understand the failure mechanisms and how they are affected by temperature. The catastrophic nature of the failure in composites and the additional limitation placed on the visual investigation of failure initiation and progression suggested a displacement-controlled mode for the tests (as opposed to the load control). This facilitates examination of specimens loaded to initial (local) failure but recovered prior to global failure. The influence of hole size on the failure mode had been established and verified before.[10,13] Therefore, in the present study, one hole size

Table 3 Cross-ply laminate experimental data

Specimen type	Temperature, C°	Loading type	Failure initiation load, ksi/MPa	Maximum hole strain, $\mu\varepsilon$	Failure mode
Cross ply	21	Uniaxial	44/303	7500	Kink at 0-deg edge
Cross ply	200	Uniaxial	19/131	2700	Kink at 0-deg edge
Cross ply	21	Biaxial	37/255	6600	Kink in 0, 90-deg edge
Cross ply	200	Biaxial	18/124	2080	Kink in 0, 90-deg edge

Table 4 Quasi-isotropic laminate experimental data

Specimen type	Temperature, C°	Loading type	Failure initiation load, ksi/MPa	Maximum hole strain, $\mu\varepsilon$	Failure mode
Quasi isotropic	21	Uniaxial	21/145	6600	Shear failure (+45/−45)
Quasi isotropic	200	Uniaxial	19/131	3900	Shear failure (+45/−45)
Quasi isotropic	21	Biaxial	26/179	4443	Shear failure (+45/−45)
Quasi isotropic	200	Biaxial	24/165	2872	Shear failure (+45/−45)

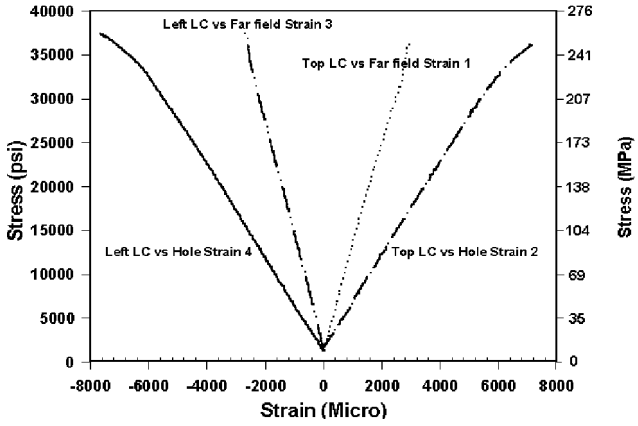

Fig. 3 Experimental strain results for equibiaxial displacement loading of a cross-ply laminate plotted against remote strain (room temperature).

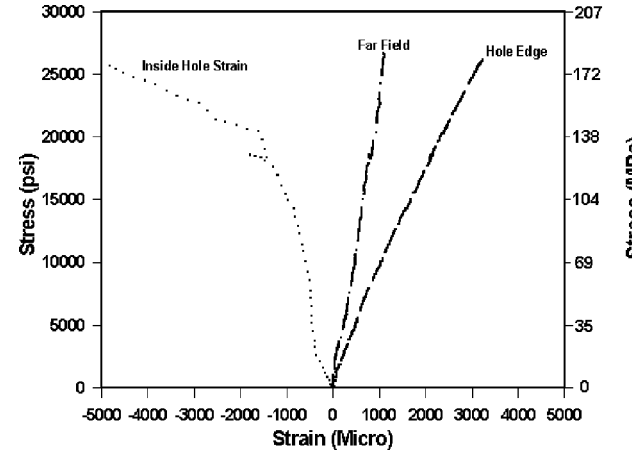

Fig. 4 Experimental strain results for a uniaxially loaded cross-ply laminate at elevated temperature.

(0.5 in. diam) was chosen for all specimens. Each test consists of loading a particular type of laminate until global failure, to estimate the ultimate strength of the specimen. This information is used subsequently to aid in unloading similar specimens that have failure initiated but that have not reached their ultimate load carrying capacity. A sudden nonlinear (with respect to a far-field load component) increase in the through-the-thickness strain inside the hole (strain gauge placed through the thickness on the hole edge) indicates that there is failure initiation at the hole edge of the specimen. At this point, there may not be a sign of global failure of the specimen.

Note that in the elevated temperature experiments, during the heating cycle, the loading piston was separated from the specimen grips initially, to ensure free thermal heating, with freedom for unconstrained thermal expansion (or contraction). Thermal strains were measured and recorded. These values were used for establishing the laminate orthotropic thermal expansion coefficients.[12]

A typical strain history is shown in Fig. 3 for a cross-ply laminate loaded in equibiaxial compression at room temperature. As expected, the response is symmetric because the cross-ply laminate has equal stiffness along the loading directions. Detecting localized failure was done by following the through-the-thickness strain, as shown in Fig. 4, for a uniaxially loaded cross-ply specimen at elevated temperature. The test was stopped as soon as any nonlinear strain increase was observed in the through-the-thickness strain reading. The unloaded specimens were sectioned and observed under an optical microscope to examine the failure initiating mechanisms. Both the in-plane and out-of-plane views of the failed region were examined and digital photomicrographswere acquired. A similar procedure was used to study the remainder of the specimens.

Room Temperature Results

The mechanism of failure in cross-ply laminates was kink banding (also identified before by a number of researchers; see Refs. 13–23). The values of far-field stress at failure for different loading conditions are indicated in Table 3. Failure initiates in the zero plies, at the hole edge, and propagates in a direction that is perpendicular to the direction of applied far-field load. Both, inplane and out-of-plane kink banding occurs in the zero plies (Fig. 5). For uniaxial loading at room temperature, the surface strain at the hole edge in the direction of applied load at failure initiation is 7500 $\mu\varepsilon$ and the corresponding far-field strain is approximately 3000 $\mu\varepsilon$. When the damage propagates in the form of kink bands, the fiber/matrix interface is completely severed in a number of fibers within the kink bands. In addition, the kink banding also introduces interlaminar separation between the kinked ply and the neighboring 90-deg plies.

Quasi-isotropic laminate specimens fail by both inplane shear failure and kink banding simultaneously (Fig. 6). Whether kink bands form in the 0-deg plies or fiber/matrix interface failure occurs in the 45-deg plies is determined by 1) the specimen characteristics (stacking sequence, fiber/matrix interface toughness, and initial fiber misalignment) and 2) the in situ shear response of the matrix. In the present case, it is possible that shear failure along the fiber/matrix interface led to catastrophic failure of the specimens. Although there was evidence of kink band formation observed after the test, the fiber/matrix interfacial failure in the 45-deg plies was seen to be extensive, starting at the hole edge and propagating outward. A summary of the critical quantities at failure of quasi-isotropic laminates is given in Table 4.

The main difference in response of the laminates between the remote uniaxial and the equibiaxial displacement loading is not in the

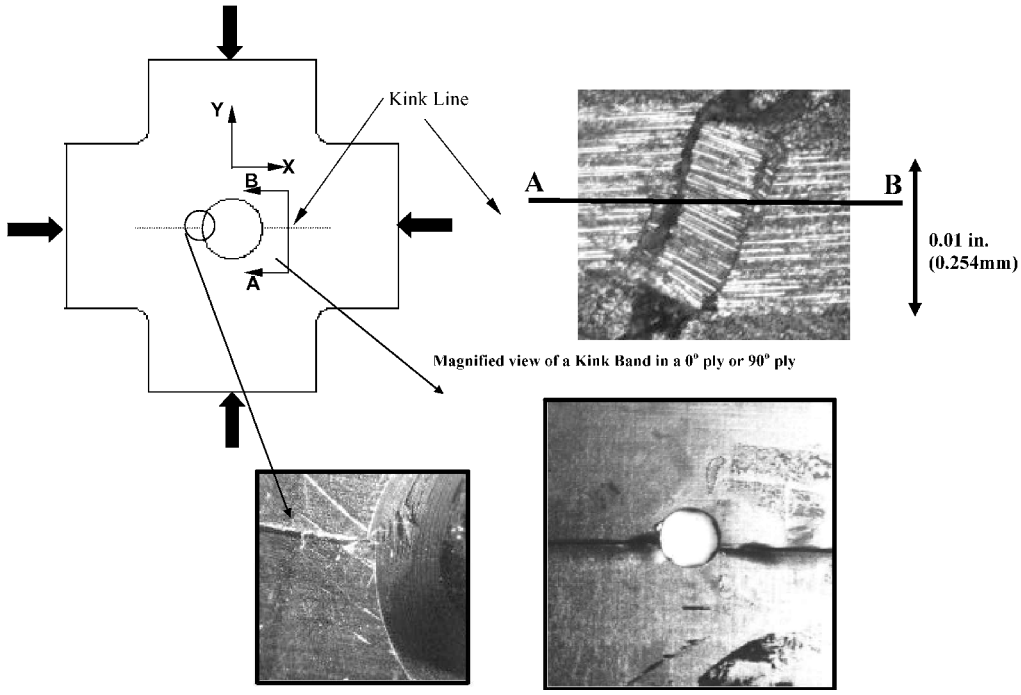

Fig. 5 Cross-ply laminate failure mechanism (biaxial, room temperature).

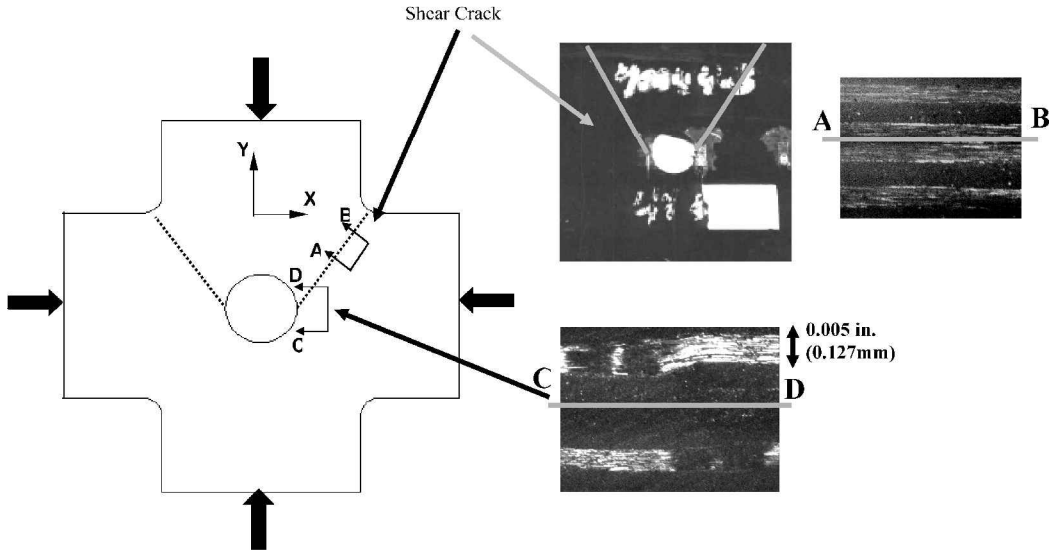

Fig. 6 Quasi-isotropic laminate failure mechanism (biaxial, room temperature).

mechanism of failure, but the magnitude of far-field loading necessary to achieve failure initiation. Remote equibiaxial compression loading tends to relieve the compressive stress gradient away from the hole, as compared with uniaxial loading. For the cross-ply case, this combined effect due to biaxial loading does not show much of an effect on the magnitude of the failure initiation stress because the failure mechanism is initiated by a fiber instability. However, the quasi-isotropic specimens show different far-field failure initiation loads depending on whether the remote loading is uniaxial or equibiaxial. This is because the failure mechanism is governed by the state of shear in the matrix, which is a strong function of ply angle and overall stacking.

In summary, in cross-ply laminates, because there are only 0-/90-deg plies, failure initiation occurs by kink banding in the 0-deg plies, starting from the hole edge at a position that is perpendicular to the direction of loading. Ideally, both kink bands (on either side of the hole) should form simultaneously, but due to material non-homogeneity or a slight perturbation of the symmetry of loading, one of the two kink bands forms first, followed by the other. The kink band formation leads to interlaminar cracking between the kinked ply and the adjacent 90-deg ply. Quasi-isotropic laminates show a competition between shear failure in the $+45/-45$ lamina and the 0/90 lamina. The experimental results show that quasi-isotropic laminates fail by interfacial failure along the ± 45-deg plies; however, it is postulated that this mechanism is triggered by kink banding in the zero plies, as modeled later.

Elevated Temperature Results

At elevated temperature, a new parameter emerges to influence the mechanism of failure. Because the matrix properties undergo degradation as temperature increases, the matrix-sensitive mechanical properties of laminates such as the instantaneous composite transverse modulus and the instantaneous composite shear modulus are affected at elevated temperature. An examination of the shear response of the in situ matrix as a function of temperature provides a convenient means to establish the manner in which matrix-sensitive

Table 5 Results of the mesh convergence with hole diameter 0.5 in. (12.7 mm)

Mesh used	Dimensions X length $\times$ Y length	Maximum imperfection size	Maximum resultant stress on microregion, kpsi/MPa	Plateau stress on microregion
Baseline	$300d_f \times 142d_f$	$1.81d_f$	37/255	29
Mesh A	$375d_f \times 142d_f$	$1.81d_f$	37/255	28
Mesh B	$300d_f \times 177d_f$	$1.81d_f$	37/255	27
Mesh C	$375d_f \times 177d_f$	$1.81d_f$	37/255	26
Mesh D	$450d_f \times 213d_f$	$1.81d_f$	37/255	29

properties are degraded with increase in temperature. Furthermore, due to the mismatch in the coefficients of thermal expansion, the nature of the fiber/matrix interface is also changed. In addition, the matrix-rich region between plies that control the interlaminar strength is also affected.

As in the room temperature tests, failure initiation is sensed by a sudden increase in the through-the-thickness (out-of-plane mode) strains, which allows the unloading of a specimen for postfailure microscopic examination of regions near the hole edge. Cross-ply laminates show extensive kink formation just as in the room-temperature case. Compared to the room-temperature case, failure occurs at a lower load (see Table 3). Again, the kink banding initiates at the hole edge and propagates in a direction perpendicular to the direction of loading (Fig. 5). Noticeably, the out-of-plane failure is very extensive. This observation may point to the reduced interlaminar strength at elevated temperature, for the reasons discussed earlier.

Quasi-isotropic laminates (Table 5) show a combination of different failure modes; however, fiber/matrix shear failure is still the dominant failure mechanism for damage propagation. A band of damage consistently propagates along the $+45/-45$ line from the 0-deg hole edge, in the form of interfacial fiber/matrix cracking, indicating that this is the form of energy release at failure.

Modeling of Compressive Response of Multiply Multidirectional Laminates

As observed in the experiments, when a multidirectional laminate containing a circular hole is subjected to remote compressive loads, failure in the form of a microstructural instability is initiated in the vicinity of the hole, which is the area of highest stress concentration. For cross-ply laminates, the failure is triggered by a 0-deg ply instability, characterized by fiber kinking. For the case of quasi-isotropic laminates, which consist of 0- and 45-deg plies, two types of failure mechanisms compete against each other. These are failure initiation due to fiber instability in the zero plies, and failure initiated by matrix shear response, responsible for interface (fiber/matrix) cracking and/or matrix shear failure. The dominant failure mode for this type of laminates has been reported as zero-ply kinking failure.[10,23] However, it is not clear whether post mortem investigation or surface imaging of a particular laminate system (fiber, matrix, and layup) can pinpoint the general failure initiation mechanism. Based on this, it was decided to investigate both possibilities of fiber kinking and matrix shear failure. Furthermore, it is hypothesized that the in-plane kinking failure mode is the dominant mode of failure for the symmetric quasi-isotropic laminates.

The cross-ply laminates (Fig. 7) were studied first, followed by the quasi-isotropic laminates (Fig. 8). Unlike the cross-ply laminates (0- and 90-deg plies), the quasi-isotropic laminates have three kinds of lamina (0-, 450- and 90-deg plies). Therefore, it is necessary to separate the two families of lamina in the region of study (the 0-/90-deg lamina and the 45-deg lamina).

The failure initiation analysis based on micromechanics is carried out in a manner similar to that described by Ahn and Waas.[23] The region of failure near the cutout and corresponding to the zero plies are isolated and analyzed using the finite element method. The size of this region is left as an unknown of the problem. A converged solution is obtained when the salient features of the micromechanics based analysis shows no difference with respect to the size of the meshed area.

For the FEA analysis, a rectangular mesh containing 22,650 elements (four-node quadrilateral plane strain) and 23,028 nodes,

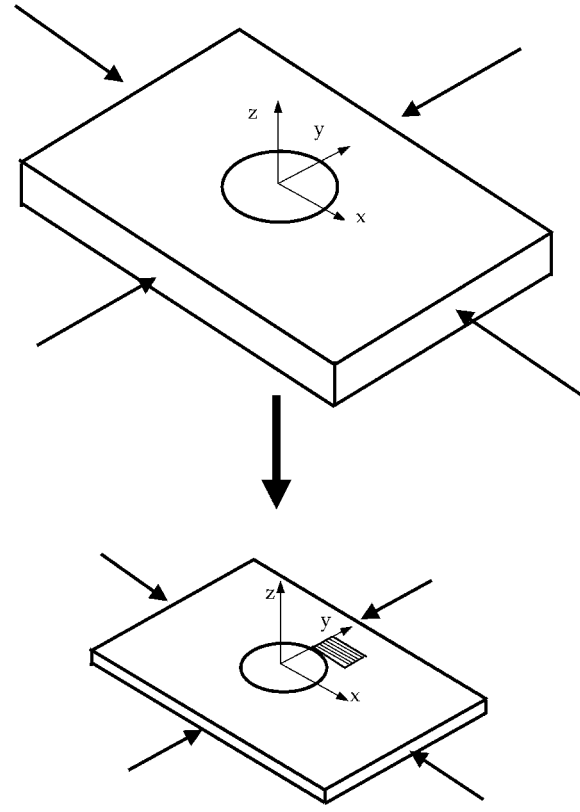

Fig. 7 Cross-ply laminate microregion for FEA.

with two degrees of freedom (u and v) per node was chosen. The ABAQUS commercial solver was used. The initial mesh size (termed baseline model) corresponds to a rectangular region that is 300 fiber diameters d_f in length and 142 fiber diameters in width. The elements were of length $2d_f$, and width $0.5d_f$, such that two layers of elements constitute a single fiber. The matrix was also modeled with two adjacent elements, albeit the two matrix elements differed in width from the two fiber elements, taking into account the difference in thickness of the matrix such that the matrix volume fraction V_m corresponds to the specimen (55%). Convergence and mesh size dependency were checked by incrementally increasing the mesh size until no substantial change in the salient features (and values) associated with the response resulted. The results of the mesh sensitivity study are shown in Fig. 9 and Table 5, for a configuration of the current analysis [hole diam 0.5 in. (12.7 mm)]. As can be seen in Table 5, the maximum limit load (our analysis uses this value as the failure initiation point) is insensitive to mesh size, and the plateau load also shows insignificant change as mesh size varies. Based on this mesh sensitivity study, the analysis model was deemed to have satisfactory convergence for the present study.

Each microregion is situated as shown in Figs. 7 and 8, where the symmetry plane ($y = 0$) is marked as indicated. The Lekhnitskii[11] solution corresponding to a notched laminate of infinite extent is used to compute the displacement fields along the edges corresponding to the microregion. These displacement fields are computed corresponding to a unit far-field load in the case of uniaxial loading and unit far-field proportional loads in the case of biaxial loading.

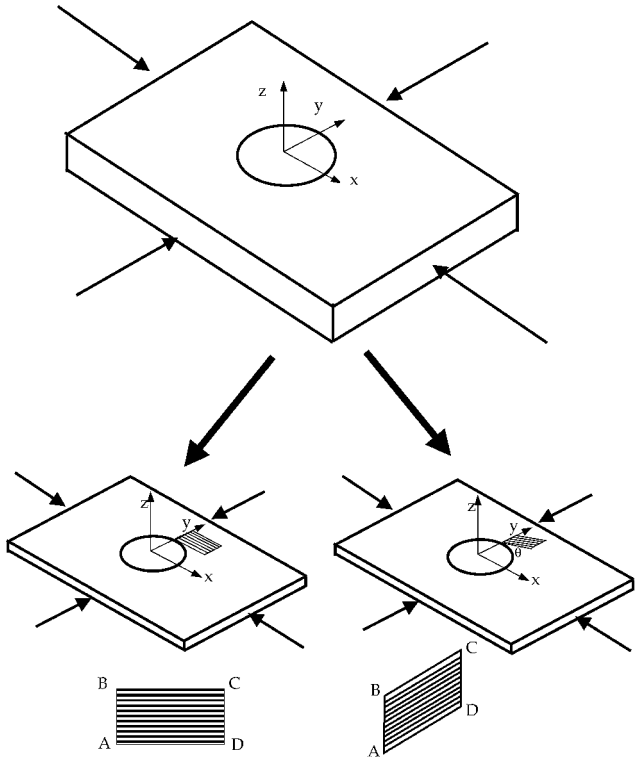

Fig. 8 Quasi-isotropic laminate microregion for FEA.

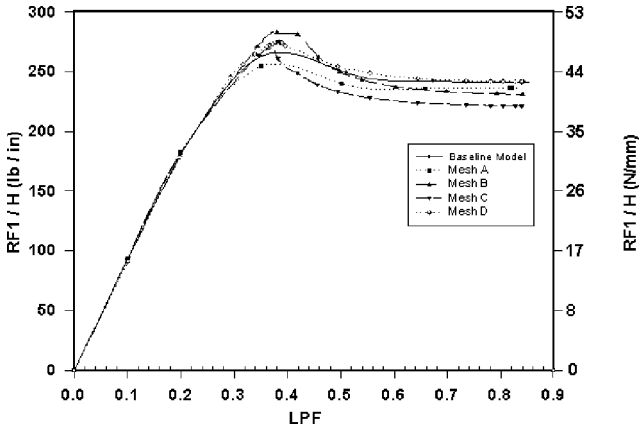

Fig. 9 Effect of mesh size on load-shortening behavior of microregion.

Along the bottom edge of the microregion (marked as *AD*), equilibrium nodal equivalent loads are enforced. That is, the edge *AD* is under load control, and the remaining edges are under displacement control, so that fibers can deform according to the requirement of far-field equilibrium. It turns out that, if an analysis is conducted with the edge *AD* free of tractions, the results obtained for the salient features associated with the deformations within this microregion do not change. This is not surprising because the dominant loading is compression along the fibers, whereas the tractions along the bottom edge (edge *AD*) of the microregion are negligible compared to these dominant compressive stresses. Nevertheless, the objective is to obtain the limit load that the microregion can sustain, as well as the corresponding far-field stresses.

A flowchart of the analysis procedure is given in Fig. 10a. First, an elastic eigenvalue analysis of the microregion is carried out to obtain the eigenmodes of the microregion. Next, by the use of the eigenmode associated with the smallest nonzero eigenvalue as a perturbation to an otherwise perfect mesh, a response analysis is carried out using the Riks method option provided in ABAQUS. This is done for a series of imperfection magnitudes. The eigenmodes provide

Table 6 Comparison of experiment and analysis for cross-ply laminate

Case	Uniaxial, ksi/MPa (21°C)	Uniaxial, ksi/MPa (200°C)	Biaxial, ksi/MPa (21°C)	Biaxial, ksi/MPa (200°C)
Analysis	62/427	30/207	67/462	35/241
$\phi \approx 0.8$ deg	40/276	21/145	46/317	25/172
Experiment	44/303	19/131	37/255	18/124

Table 7 Comparison of experiment and analysis for quasi-isotropic laminate

Case	Uniaxial, ksi/MPa (21°C)	Uniaxial, ksi/MPa (200°C)	Biaxial, ksi/MPa (21°C)	Biaxial, ksi/MPa (200°C)
Analysis	38/262	22/152	44/303	24/165
$\phi \approx 0.8$ deg	27/186	15/103	34/234	18/124
Experiment	21/145	19/131	26/179	24/165

the perturbation shape, but not the absolute magnitude of perturbation. Thus, the user must specify the imperfection magnitude. In the present work, this is achieved as follows: As shown in Fig. 10b, the maximum amplitude of the lowest eigenmode (which occurs along the edge *AD*) is chosen such that the fiber misalignment angle ϕ is approximately in the range 0.05–1 deg. Because λ is known, δ is chosen such that ϕ assumes the intended value. After several runs corresponding to different values of ϕ are completed, the load maxima associated with the resultant compressive load on edge AB of the microregion or reaction force (RF1) vs the load proportionality factor (LPF) (fraction of the total applied load) curves are plotted as a function of imperfection magnitude. Then, by extrapolation, the value corresponding to the perfect case (no imperfection) is obtained. The perfect case corresponds to perfectly straight fibers, and this case yields an upper bound for the attainable load maximum. The perfect case was also analyzed separately (with straight fibers) as a nonlinear response problem, and it yielded the same result for the maximum load and plateau load as that obtained by extrapolation. As shown by Ahn and Waas,[23] the present problem is one where the loading on the microregion boundaries is nonunifrom. As a result, this load nonuniformity essentially produces the same effect as that of an initial geometrical imperfection of the fibers (such as fiber misalignment). Therefore, even in the absence of an initial fiber misalignment, the perfect microregion response analysis exhibits a limit load type behavior.

The fiber (IM7) is assumed to be linearly elastic (see Table 1), and the matrix (3270 toughened epoxy) property within the laminate is evaluated from the $+45/-45$ coupon test, which will be described in the next section. The matrix is modeled as a $J2$ incremental flow theory solid with isotropic hardening. Thus, the in situ elastic-plastic matrix behavior is incorporated in the present analysis.

The cases studied herein correspond to those from the experiments reported earlier. Thus, for each laminate, two different runs are performed, one at room temperature and one at elevated temperature. For each temperature, uniaxial and biaxial loading cases are investigated. In this manner, we have studied four different cases for each laminate type. Of course, in the quasi-isotropic case, there are four additional cases because both the zero ply and the 45-deg ply are investigated. Tables 6 and 7 show results corresponding to the preceding cases. The results obtained for different imperfection magnitudes are also shown in Tables 6 and 7.

In Situ Matrix Characterization

To evaluate the material properties of the matrix within the laminate (in situ matrix properties), a $(\pm 45)_{ns}$ coupon test (Fig. 11) at room and high temperature was performed following the procedure of American Society for Testing and Materials ASTM-D3518-76 (Ref. 24). The elastic properties of the lamina and the complete shear-stress/shear-strain behavior of an IM7/3270 in the principal material coordinate system were obtained from this test. The procedure used to generate the data consists of subjecting a $(\pm 45)_{ns}$ angle ply laminate to uniaxial compression and measuring

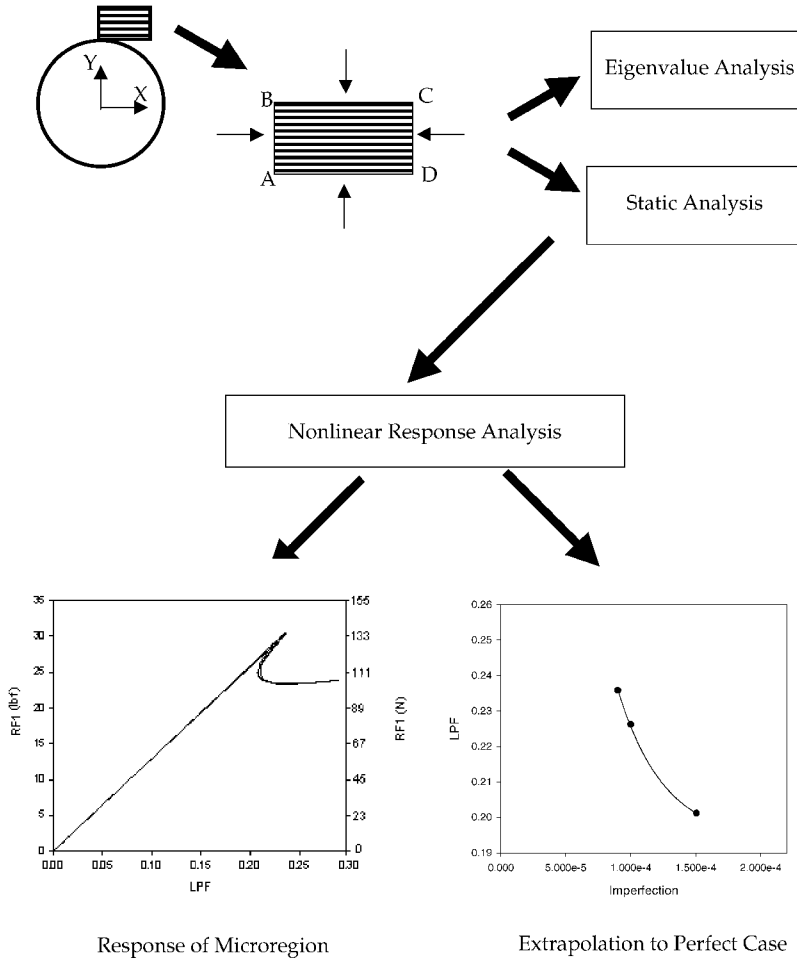

Fig. 10a Imperfection sensitivity analysis procedure.

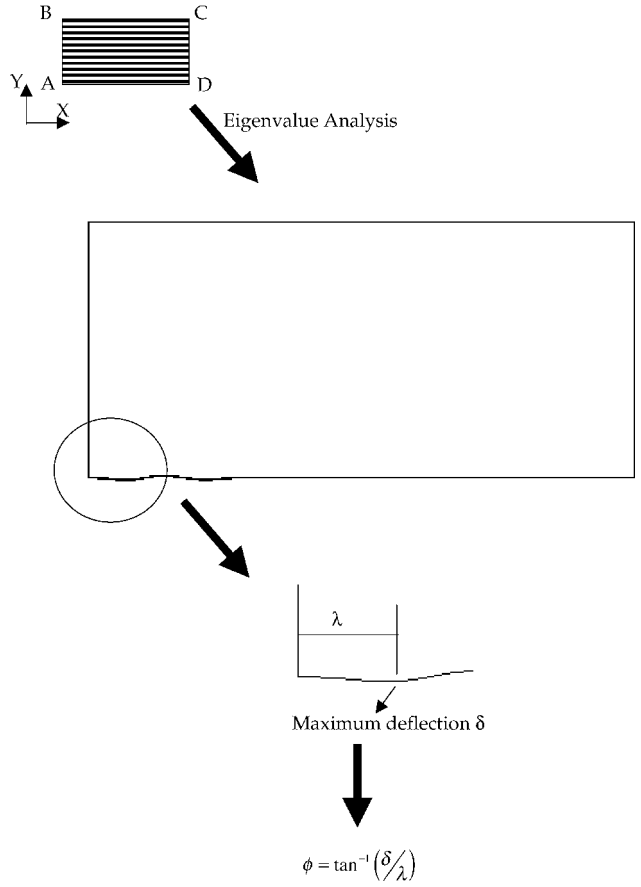

Fig. 10b Imperfection magnitude definition based on ϕ (maximum deflection angle).

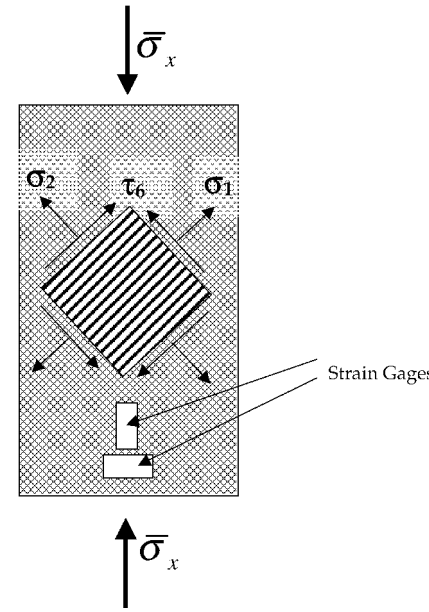

Fig. 11 The +45/− 45 coupon test of a specimen taken from the cross-ply laminate.

the laminate strains ε_{xx} and ε_{yy} and the applied remote stress on the laminate. Note that, for this test, $\gamma_{xy} = \varepsilon_{xx} - \varepsilon_{yy}$. The data shown in Fig. 12 from this test can be used to extract the complete nonlinear shear-stress/shear-strain response of the in situ matrix (3270) as discussed hereafter. We begin by assuming that the 3270 matrix material can be modeled as an elastic–plastic solid obeying the small strain $J2$ flow theory of plasticity.[25] Then, from the elastic (linear) portion of the curve in Fig. 12, we first obtain the in-plane lamina

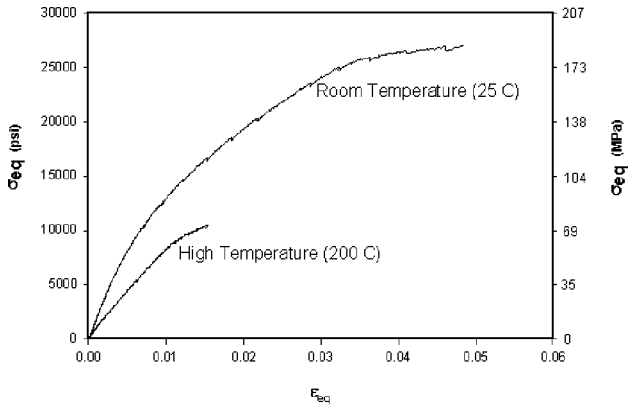

Fig. 12 The +45/− 45 compression experiment result.

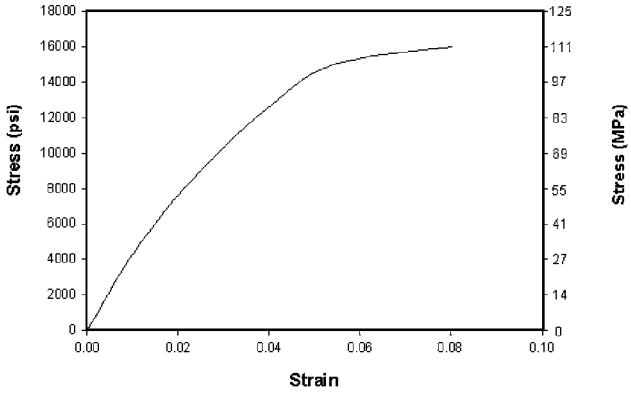

Fig. 13 Shear stress τ_{12} vs shear strain γ_{12} curve for IM7/3270 (room temperature) based on *J*2 flow theory of plasticity and the data in Fig. 12.

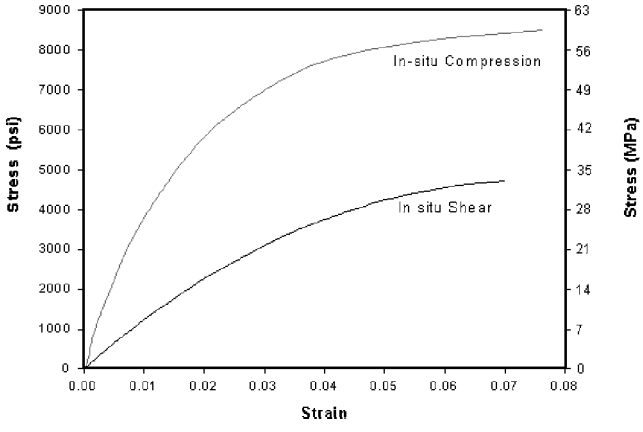

Fig. 14 In situ shear stress vs shear strain response of the matrix and the deduced uniaxial stress vs uniaxial strain response of the matrix (room temperature).

shear modulus G_{12}. In the lamina principal coordinates, we know that

$$\varepsilon_{11} = \varepsilon_{22} = (\varepsilon_{xx} + \varepsilon_{yy})/2, \qquad \gamma_{12} = 2\varepsilon_{12} = \varepsilon_{xx} - \varepsilon_{yy} \quad (1)$$

$$\sigma_{11} = \sigma_{xx}/2, \qquad \sigma_{22} = \sigma_{xx}/2, \qquad \tau_{12} = \sigma_{xx}/2 \quad (2)$$

Thus, using Eqs. (1) and (2) and the definitions of equivalent stress $\bar{\sigma}$ and equivalent plastic strain increment $d\bar{\varepsilon}^p$ (in the Appendix), the data in Fig. 12 can be used to construct a plot of $\bar{\sigma}$ against $\bar{\varepsilon}^p$.

According to the $J2$ flow theory of plasticity with a Mises–Henky yield condition, the ratio of the increment of each plastic strain component to its corresponding deviatoric stress component remains constant, which is (see Ref. 25)

$$d\varepsilon_{ij}^p \big/ \hat{\sigma}_{ij} = d\lambda \quad (3)$$

Using Eq. (3), and the relation between $\bar{\sigma}$ and $d\bar{\varepsilon}^p$, the nonlinear portion of the shear-stress τ_{12}/shear-strain γ_{12} response curve for a single lamina can be extracted. The curve thus obtained for IM7/977-3 system is shown in Fig. 13. The instantaneous slope of the curve in Fig. 13 is the tangent shear modulus of the lamina $G_{12}(\tau_{12})$. Therefore, we next use the approximate Halpin–Tsai relations (see Ref. 26) to extract the variation of the in situ matrix shear modulus $G_m(\tau_{12})$ by using $G_m(\tau_{12})$,

$$G_m = G_{12}\left(\frac{1 + \xi_2 \cdot \eta_2 \cdot v_f}{1 - \eta_2 \cdot v_f}\right)^{-1}, \qquad \eta_2 = \frac{G_{12f} - G_m}{G_{12f} + \xi_2 G_m} \quad (4)$$

and $\eta_2 = 1$ for random packing of fibers. With $G_m(\tau_{12})$ so obtained, the in situ matrix shear-stress/shear-strain curve is as shown in Fig. 14. In a similar manner, the in situ uniaxial stress/strain curve in

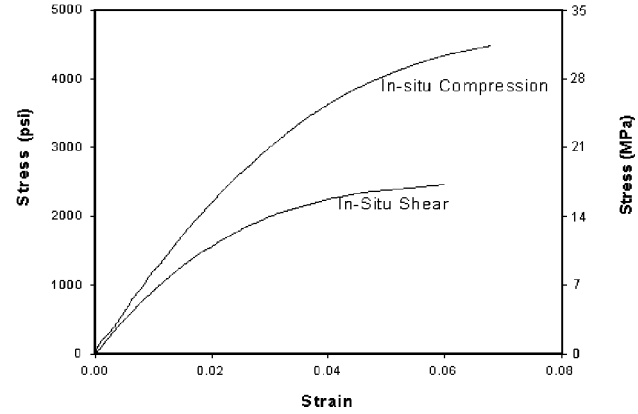

Fig. 15 In situ shear stress vs shear strain response of the matrix and the deduced uniaxial stress vs uniaxial strain response of the matrix (high temperature).

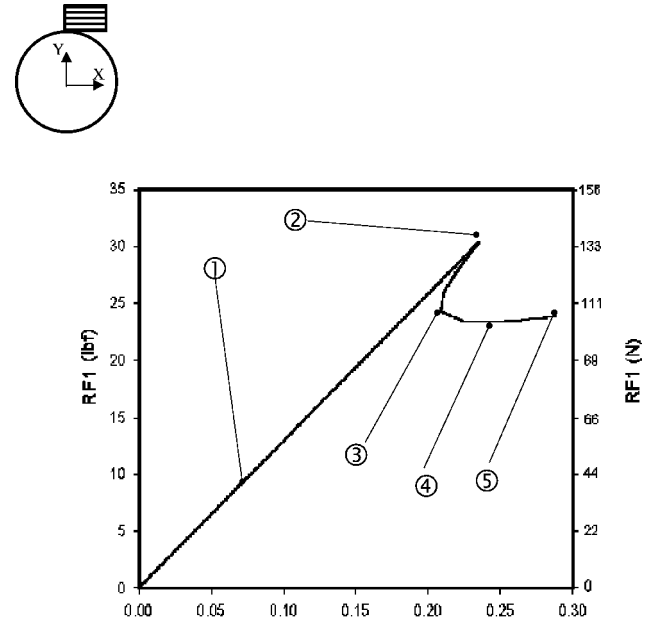

Fig. 16 Typical microregion response plot of cross-ply laminate.

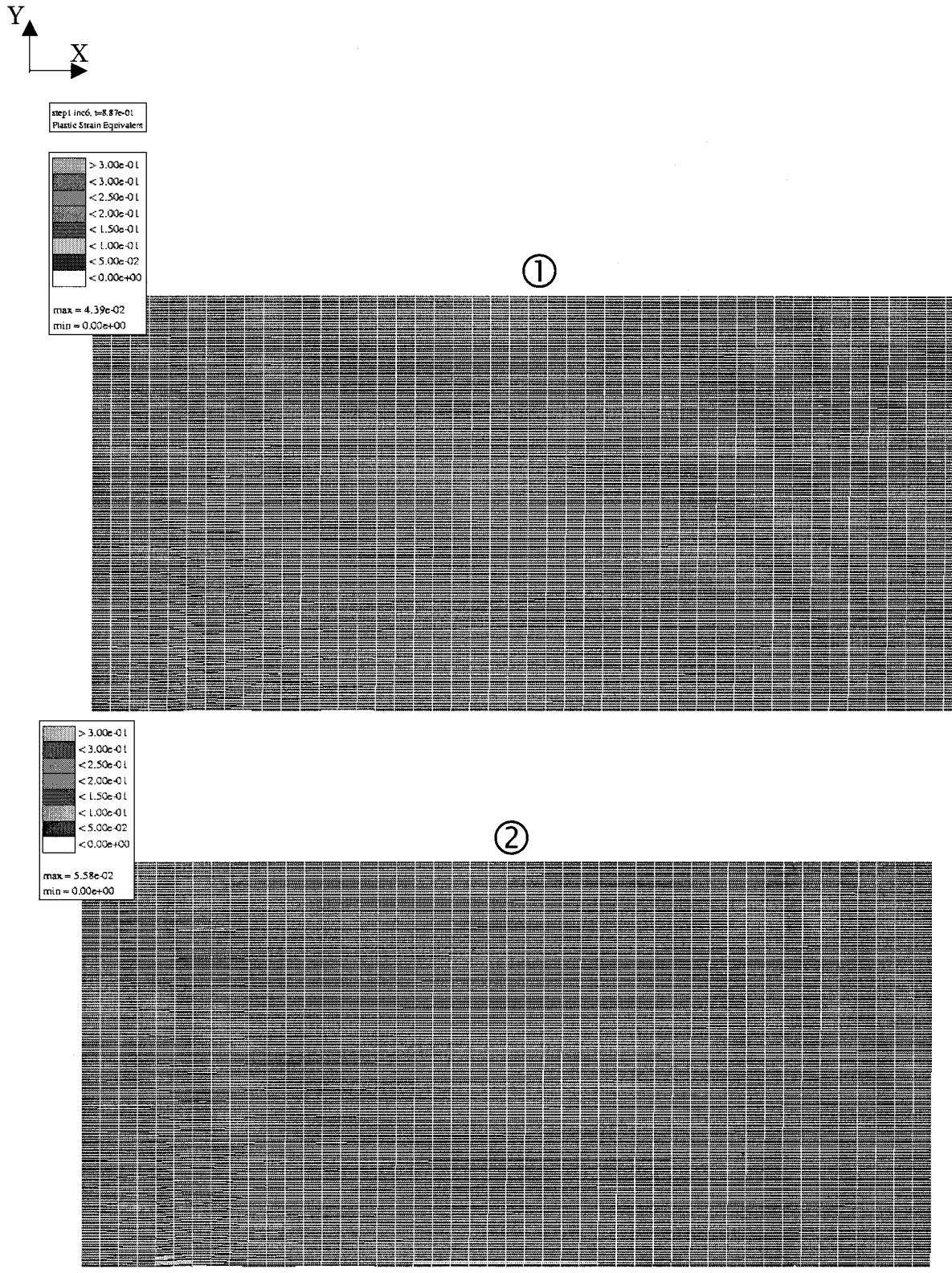

Fig. 17 Deformed microregion shape (equivalent plastic strain contour plot).

compression for the matrix is also obtained. This uniaxial response curve was used in the input data file for the micromechanics based FEA. This curve is also shown in Fig. 14. The same procedure is applied to the high temperature case, and the results obtained for the matrix stress/strain curves are shown in Fig. 15.

FEA Results and Interpretation

A typical load response behavior of a microregion within a cross-ply laminate model is shown in Fig. 16, and a series of deformed plots of the microregion showing the initiation and propagation of damage in the form of kink banding is shown in Fig. 17. The numbers indicated in Fig. 16 correspond to the series of deformation plots shown in Fig. 17. The microregion response follows a linear path up to point ①. Although local matrix yielding (in areas of the microregion near the cutout) is indicated before the attainment of point ②, the total integrity of this region is not affected much from the matrix yielding because 1) the area of yielding is small compared to the overall size of the microregion and 2) the fiber rotation is small up to the point of maximum load (point ②). Thus, the resultant RF1 vs LPF relation is linear up to the maximum load point, although this

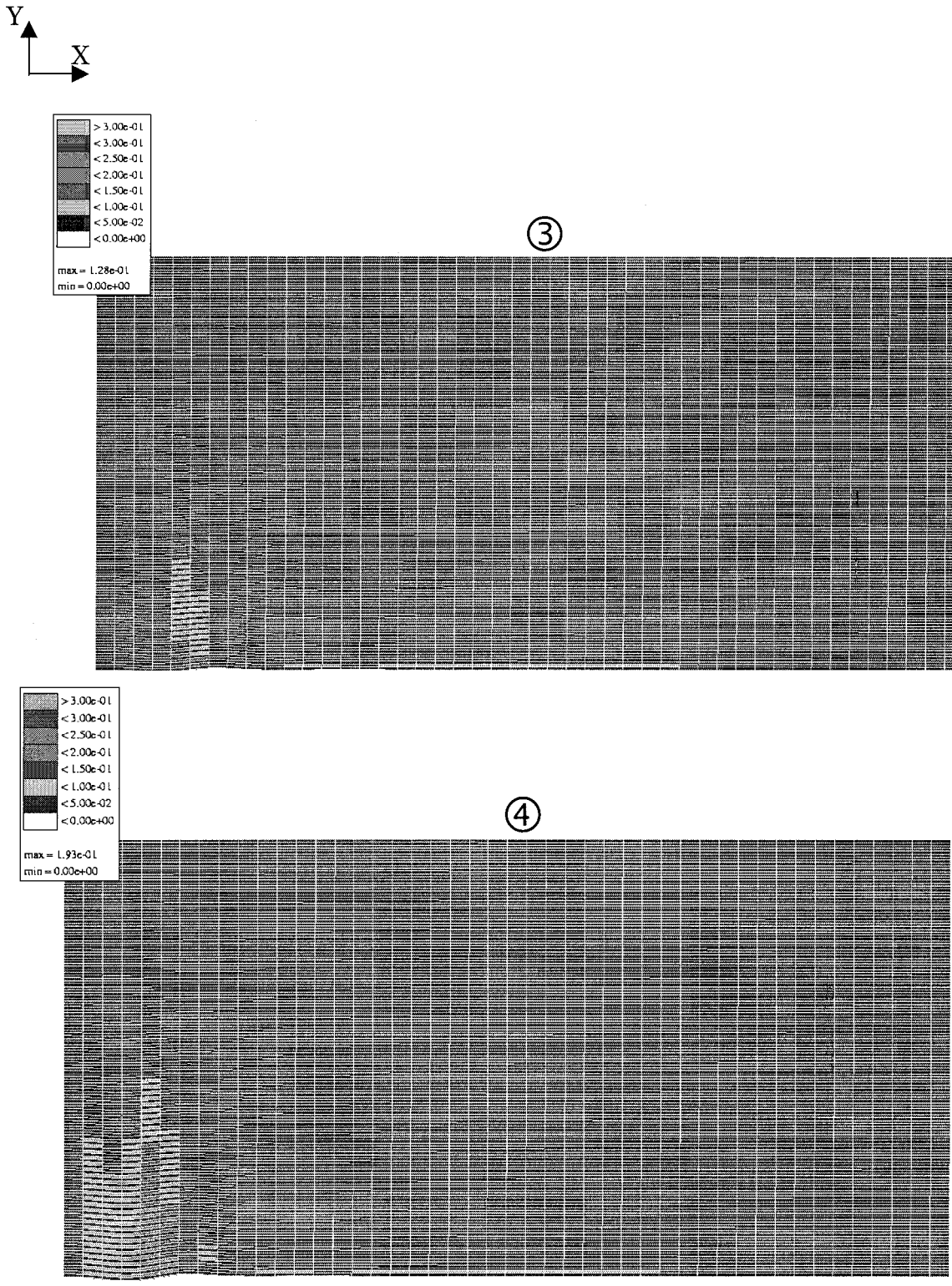

Fig. 17 Deformed microregion shape (equivalent plastic strain contour plot) (continued).

is not necessarily what could be expected; that is, in general the RF1 vs LPF behavior is problem dependent. As loading increases, the fibers in the areas where the matrix has become softer start to rotate, resulting in a drop of the resultant RF1 computed at the symmetry plane (indicated by point ③ in Fig. 11). As deformation progresses, the region of matrix yielding (and corresponding fiber rotation) is expanding, propagating upward away from the areas near the cutout (until it reaches point ④; see Fig. 11 for the deformed configuration). Once the region expands away from the hole to an area where the effect of the stress gradient has diminished, there is no tendency for further propagation, and, thus, the load assumes a fairly constant value (plateau load). After this point, deformation becomes stabilized (fiber rotation stops), and the band of kinked fibers starts to broaden in the x direction without any further sudden drop in the reaction force (⑤). The scenario just described is quite typical of the response of the microregions for all of the cases corresponding to the cross-ply laminate as well as to the zero-ply microregion within a quasi-isotropic laminate. The far-field load (or loads corresponding to biaxial tests) corresponding to point ② is read off and tabulated in Table 1 for all of the cross-ply laminate cases studied herein.

For the case of quasi-isotropic laminates (Fig. 2), the responses look different for each lamina (0 ply and 45 ply). Again, the zero-ply

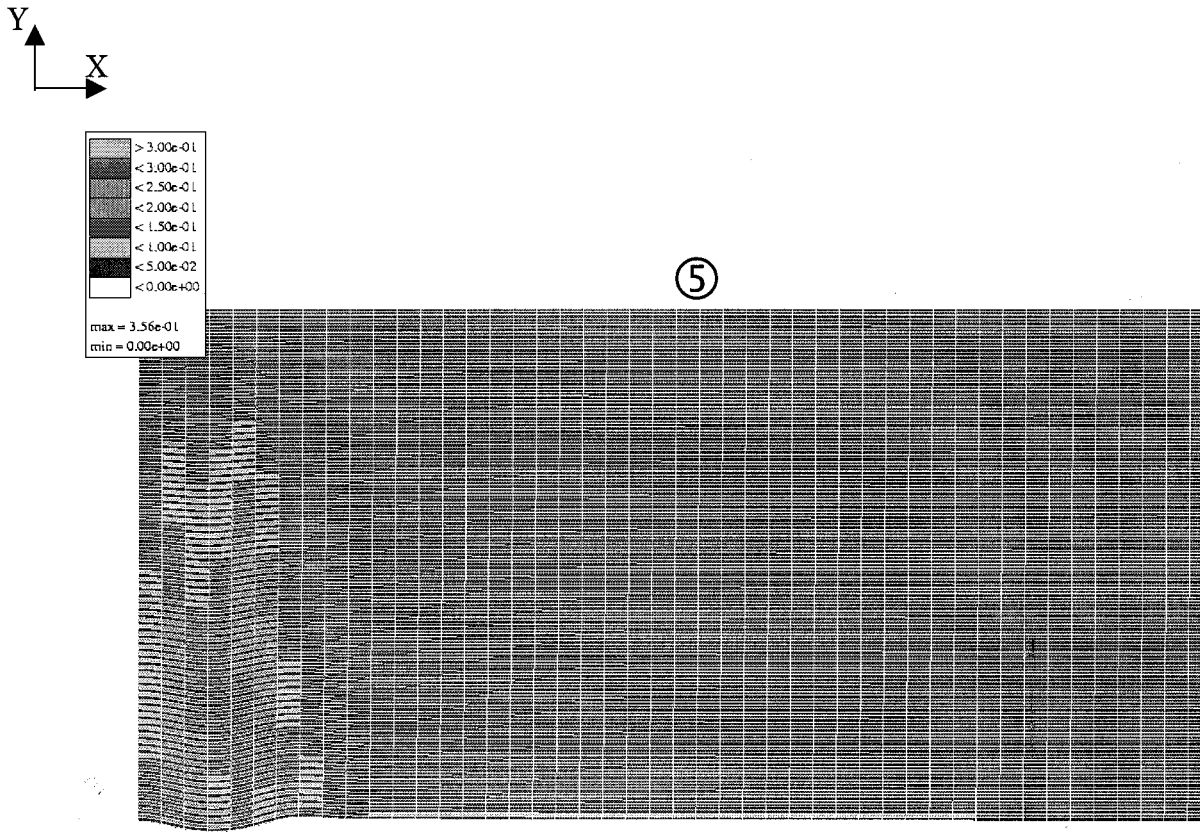

Fig. 17 Deformed microregion shape (equivalent plastic strain contour plot) (continued).

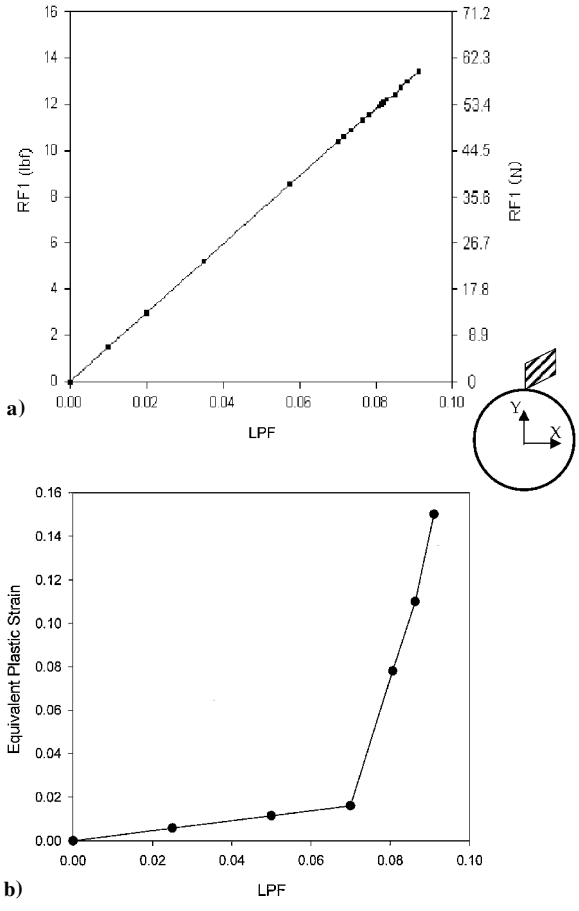

Fig. 18 Microregion response result for a quasi-isotropic laminate, 45-deg ply. { The equivalent plastic strain is sampled at the point with coordinate [0.021 in. (0.533 mm), 0.271 in. (6.88 mm)].}

response is similar to that of the cross-ply model, but the far-field load at which kink banding initiates is different. The 45-deg ply is modeled in a manner that is similar to the zero-ply microregion, but the microregion boundaries are taken to be along the material principal directions (in this case the 45- and 135-deg directions, see Fig. 8). Again, displacement boundary conditions are enforced on the edges *AB*, *BC*, and *CD*, whereas edge *AD* is subject to equivalent equilibrium nodal loads. As loading proceeds, the RF1 vs LPF relation is very nearly linear (Fig. 18a) and shows no sign of leading to a load maximum preceding a sudden load drop. At the same time, the corresponding plots for the equivalent plastic strain ε^p vs LPF [Fig. 18b, sampled at the location with coordinates (0.025 in., 0.276 in.)] shows that the matrix elements contained between any two fibers along the 45-deg direction and close to the cutout undergo increasing amounts of shearing. As loading proceeds, more and more of the matrix elements undergo large amounts of shearing. Simultaneously, the RF1 vs LPF plot for the zero-ply microregion approaches a maximum load. Thus, the scenario is as follows: the zero-ply reaches a maximum load, at which stage kink banding is about to initiate in this ply. At the same time, the integrity of the 45-deg ply is compromised due to the large amounts of plastic straining. Thus, the laminate has a choice in selecting the failure path that corresponds to the largest release of energy. As observed experimentally, a fiber/matrix interfacial crack is seen to dominate the failure within the 45-deg ply but not without some incident kink banding in the zero plies. Therefore, for quasi-isotropic laminates, the maximum load corresponds to the initiation of kink banding that then triggers the mode of fiber/matrix interfacial failure that is observed experimentally in the 45-deg plies. Clearly, we need to have an accurate knowledge and measurement of the critical fiber/matrix interfacial fracture toughness (or the in situ matrix fracture toughness because the crack meanders between the fiber matrix interface and along the matrix) to carry out a fracture mechanics based energy release rate analysis of the 45-deg ply. Such an analysis will determine the mode of failure for which the largest amount of energy is released. A fracture mechanics based analysis is relegated to the future, but details of such an analysis in the context of double

cantilever beam specimens is reported by Song and Waas.[27] For now, we observe the good agreement between the far-field load corresponding to the maximum load prediction and the experimentally measured failure loads as indicated in Table 3, especially for the case of small imperfection ($\phi = 0.8$ deg). This lends confidence to our contention that zero-ply kinking is the dominant and, hence, governing mode of failure initiation in notched quasi-isotropic laminates.

Conclusions

Experimental results of a series of uniaxial and equibiaxial in-plane compressive loading experiments on notched composite laminated plates under room temperature and elevated temperature conditions were presented in this paper. Two types of 48-ply graphite/epoxy composites were studied to understand their compressive failure mechanisms. The laminate stacking sequence was selectively designed to isolate the different failure mechanisms that operate in angle plies and plies oriented in the loading direction. In the specimens containing plies along the direction of the load (cross ply), uniaxial compression leads to fiber kink banding. This same scenario persists at both room and elevated temperatures.

The failure of the quasi-isotropic laminates involves a combination of kink banding and fiber/matrix interfacial failure. The magnitude of remote failure initiation loads between the loading cases (uniaxial or biaxial) at a given temperature is unlike that of cross-ply laminates. The interfacial failure persists either at $+\theta$ or $-\theta$ angle or both. Fibers crossing the line of failure were broken due to the large amount of energy released as the interfacial crack propagates rapidly. At an elevated temperature, the same failure mechanisms persist, but at different magnitudes of far-field loading. Under equibiaxial compression, the remote load to initiate failure at a given temperature is higher than the uniaxial case, whereas for cross-ply laminates there is no appreciable increase in load between the uniaxial and biaxial cases at a given temperature. Furthermore, for a given loading (uniaxial or biaxial), the failure initiation load decreases for cross-ply laminates, whereas there is not a noticeable decrease for the quasi-isotropic laminates.

From the observed results, and the loads reported in Tables 3–5, the following is concluded. In cross-ply laminates there is a noticeable decrease in the failure initiation loads between room and high temperature, whereas such a reduction is hardly noticeable in the quasi-isotropic laminates. This observation shows that the mechanism of failure initiation in cross-ply laminates (fiber instability followed by kink banding) is strongly influenced by the matrix because the mechanical properties of the matrix have been degraded at high temperature.

On the other hand, the mechanism of failure initiation in quasi-isotropic laminates is not affected as much as cross-ply laminates by temperature. It is seen that at a given temperature, biaxial loading reduces the failure initiation load for cross-ply laminates, whereas for quasi-isotropic laminates this trend is reversed.

Results from a micromechanics-based global-local FEA were used to understand the experimental results. Cross-ply laminates have only 0- and 90-deg lamina, and the majority of load is carried by simple compression of these laminae. These laminas fail by fiber microbuckling (on account of a gradually weakening matrix in shear), which in turn progresses to kink band formation due to fiber rotation, followed by band broadening and the triggering of failure in other plies.

For the quasi-isotropic laminate, the majority of the load is still carried by the zero-ply lamina. However, the difference between this laminate and the cross-ply laminate is the angled ply (45-deg ply in this case). This 45-deg ply acts as a buffer zone (lower stiffness, but better shear response). Based on the micromechanics-based FEA results, it is possible to postulate that although the matrix layers between any fibers and situated near the zone of large stress and strain gradient are undergoing excessive plastic deformation, the integrity (catastrophic failure) of the laminate is still controlled by the state of stress and deformation of the zero plies. As soon as the zero ply reaches an instability limit, two possibilities are encountered. Either energy is released by the spreading of the kink band within the zero plies or through interfacial fiber/matrix failure within the now compromised 45-deg plies. The winner of this competition is governed by the fiber/matrix interfacial fracture toughness and/or the in situ matrix fracture toughness compared against the zero-ply kink band toughness (defined as the energy released per unit advancement of the kinked band). It is probable that kink banding triggers interfacial failure because until the zero ply undergoes a load drop, the coexisting 45-deg ply has no possibility of initiating the fiber/matrix interfacial failure. Thus, the failure load prediction based on the zero-ply maximum loads provides a good agreement with the corresponding experimental data, in both cross-ply and quasi-isotropic laminates.

Appendix: Effective Stress and Effective Plastic Strain Increment

$$\bar{\sigma} = \sqrt{\tfrac{1}{2}\left[(\sigma_{11}-\sigma_{22})^2 + (\sigma_{22}-\sigma_{33})^2 + (\sigma_{33}-\sigma_{11})^2\right] + 3\left(\tau_{12}^2 + \tau_{23}^2 + \tau_{31}^2\right)}$$

$$d\bar{\varepsilon}^p = \sqrt{\left\{\tfrac{2}{9}\left[\left(d\varepsilon_{11}^p - d\varepsilon_{22}^p\right)^2 + \left(d\varepsilon_{22}^p - d\varepsilon_{33}^p\right)^2 + \left(d\varepsilon_{33}^p - d\varepsilon_{11}^p\right)^2\right] + \tfrac{4}{3}\left[d\varepsilon_{12}^{p^2} + d\varepsilon_{23}^{p^2} + d\varepsilon_{31}^{p^2}\right]\right\}}$$

Acknowledgments

The authors are grateful for financial support from the Air Force Office of Scientific Research for the initial phases of this project. The supply of the laminates at reduced cost from Fiberite (courtesy of Anthony Bosch) is acknowledged with thanks.

References

[1] Ashby, M. F., and Jones, D., *Engineering Materials 2*, Pergamon, Oxford, 1994.

[2] Mathews, F. L., and Rawlings, R., *Composite Materials: Engineering and Science*, Chapman and Hall, London, 1994.

[3] Waas, A. M., and Schultheisz, C. R., "Compressive Failure in Composites, Part II," *Progress in Aerospace Science*, Vol. 32, 1995, pp. 43–78.

[4] Starnes, J., Rhodes, M. D., and Williams, J. G., "Effect of Impact Damage and Holes on the Compressive Strength of a Graphite/Epoxy Laminate," *Nondestructive Evaluation and Flaw Criticality for Composite Materials*, edited by R. B. Pipes, STP 696, American Society for Testing and Materials Philadelphia, 1979, pp. 145–171.

[5] Sandhu, R. S., "Nonlinear Behavior of Unidirectional and Angle Ply Laminates," *Journal of Aircraft*, Vol. 13, No. 2, 1976, pp. 104–111.

[6] Daniels, J. A., Palazotto, A., and Sandhu, R. S., "Failure Charcateristics in Thermoplastic Composite Laminates due to an Eccentric Circular Discontinuity," *AIAA Journal*, Vol. 29, No. 5, 1991, pp. 830–837.

[7] Soutis, C., Fleck, N., and Smith, F., "Failure Prediction Technique for Compression Loaded Carbon Fiber–Epoxy Laminate with an Open Hole," *Journal of Composite Materials*, Vol. 25, 1991, pp. 1476–1498.

[8] Martin, R. J., Sandhu, R. S., and Palazotto, A., "Experimental and Analytical Comparisons of Failure in Thermoplastic Composite Laminates," *Experimental Mechanics*, Vol. 34, No. 1, 1994, pp. 53–65.

[9] Wham, B., and Palazotto, A., "An Investigation of Graphite PEEK Composite Under Compression with a Centrally Located Circular Discontinuity," *Composite Structures*, Vol. 35, No. 4, 1996, pp. 375–386.

[10] Khamseh, A., and Waas, A., "Failure Mechanisms of Composite Plates with a Circular Hole Under Remote Biaxial Planar Compressive Loads," *Journal of Materials and Technology*, Vol. 119, 1997, pp. 56–64.

[11] Lekhnitskii, S., *Theory of Elasticity of an Anisotropic Body*, Godden–Day, 1968.

[12] Ahn, J. H., "Failure Mechanisms of Notched Laminated Composites Under Remote Compressive Loading at Room and Elevated Temperature,"

Ph.D. Dissertation, Dept. of Aerospace Engineering, Univ. of Michigan, Ann Arbor, MI, 1999.

[13] Khamseh, A., and Waas, A., "Failure Mechanisms in Uniply Composite Plates Under Uniaxial Compression," *Journal of Materials and Technology*, Oct. 1992, pp. 304–310.

[14] Ahn, J. H., and Waas, A., "Micromechanics Based Predictive Model for Damage Initiation in Compressively Loaded Angle Ply Composite Laminates," *AIAA Journal*, Vol. 38, No. 12, 2000, pp. 2299–2304.

[15] Grape, J., and Gupta, V., "Failure in Carbon/Polyamide Laminates Under Biaxial Compression," *Journal of Composite Materials*, Vol. 29, No. 14, 1995, pp. 1850–1872.

[16] Waas, A., and Babcock, C. D., "Observation of the Initiation and Progression of Damage in Compressively Loaded Composite Plates Containing a Cutout," GALCIT SM Rept. 86-34, 1986.

[17] Waas, A., and Babcock, C. D., GALCIT SM Rept. 85-12, 1985.

[18] Waas, A., "Compression Failure of Fibrous Laminated Composites in the Presence of Stress Gradients: Experiment and Analysis," Ph.D. Dissertation, California Inst. of Technology, Pasadena, CA, 1988.

[19] Waas, A., Babcock, C. D., and Knauss, W. G., "An Experimental Study of the Compression Failure of Fibrous Laminated Composites in the Presence of Stress Gradients," *International Journal of Solids and Structures*, Vol. 26, Nos. 9/10, 1990, pp. 1071–1098.

[20] Guynn, E. G., and Bradley, W. L., "A Detailed Investigation of the Micromechanisms of Compressive Failure in Open Hole Composite Laminates," *Journal of Composite Materials*, Vol. 23, May 1989, pp. 479–504.

[21] Soutis, C., and Fleck, N. A., "Static Compression Failure of Carbon Fiber T800/924C Composite Plate with a Single Hole," *Journal of Composite Materials*, Vol. 24, 1990, pp. 536–558.

[22] Soutis, C., Fleck, N., and Smith, F., "Failure Prediction Technique for Compression Loaded Carbon Fiber-Epoxy Laminate with an Open Hole," *Journal of Composite Materials*, Vol. 25, 1991, pp. 1476–1498.

[23] Ahn, J. H., and Waas, A. M., "Finite Element Model for Compressive Failure of Notched Uniply Composite Laminates Under Remote Biaxial Loads," *Journal of Engineering Materials and Technology*, Vol. 121, July 1999, pp. 360–366.

[24] "D 3410-75 Standard Test Method for Compressive Properties of Unidirectional or Cross-Ply Fiber-Resin Composites," *Annual Book of ASTM Standards, Part 36*, American Society for Testing and Materials, Philadelphia, 1982, pp. 872–880.

[25] Lubliner, J., *Plasticity Theory*, Prentice–Hall, Upper Saddle River, NJ, 1998.

[26] Daniel, I. M., and Ishai, O., *Engineering Mechanics of Composite Materials*, Oxford Univ. Press, New York, 1994.

[27] Song, S. J., and Waas, A., "Energy Method Based Model for Mixed Model Failure of Laminated Composites," *AIAA Journal*, Vol. 33, No. 4, 1995, pp. 739–745.

A. N. Palazotto
Associate Editor